Electronic Supplementary Material (ESI) for Nanoscale Advances.

Rational design of C_2N-based type-II heterojunctions for overall photocatalytic water splitting

Xu Zhang, An Chen, Zihe Zhang, Menggai Jiao, Zhen Zhou*

School of Materials Science and Engineering, National Institute for Advanced Materials, Institute of New Energy Material Chemistry, Computational Centre for Molecular Science, Nankai University, Tianjin 300350, P. R. China

*Corresponding Authors. Email: zhouzhen@nankai.edu.cn (Z.Z.)

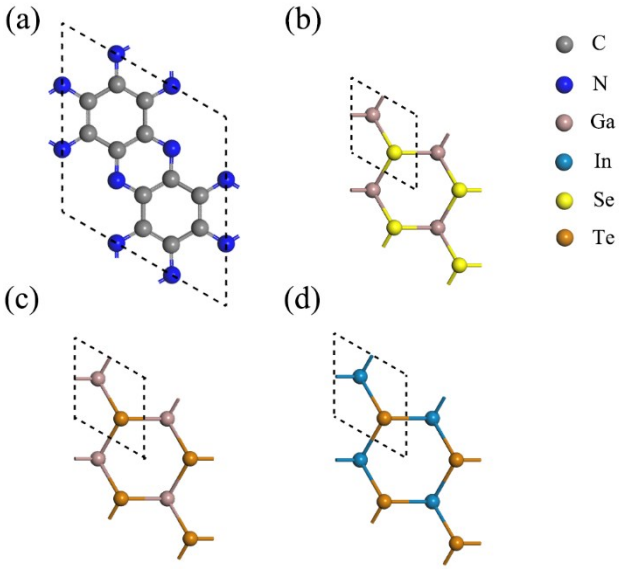

Fig. S1 Optimized geometric structures for (a) C_2N, (b) GaSe, (c) GaTe and (d) InTe. The areas circulated by dashed lines represent the unit cell.

Table S1. Lattice parameters (a = b) (Å) for C_2N, GaSe, GaTe and InTe.

	a
C_2N	8.32
GaSe	3.77
GaTe	4.09
InTe	4.32

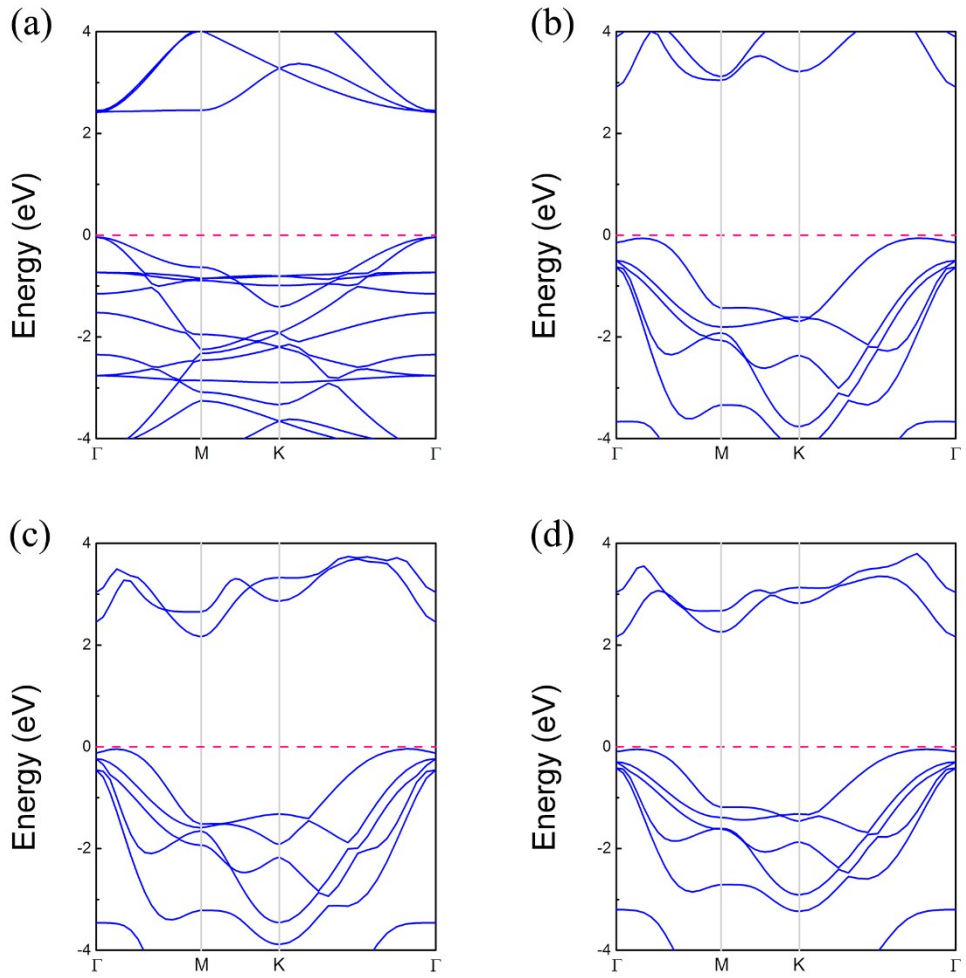

Fig. S2 Electronic band structures of (a) C_2N, (b) GaSe, (c) GaTe and (d) InTe monolayers.

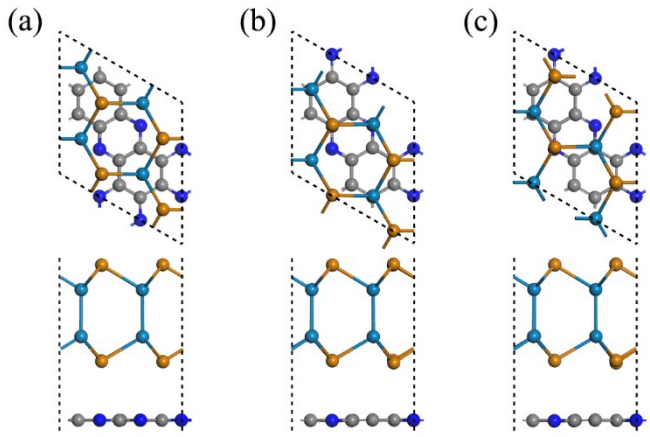

Fig. S3 Top and side view of three possible stacking patterns for C_2N/MX heterojunctions.

Table S2. Relative binding energies (eV) of three stacking patterns for C_2N/MX heterojunctions.

	a	b	c
C_2N/GaSe	0	0.13	0.08
C_2N/GaTe	0	0.11	0.09
C_2N/InTe	0	0.11	0.10

Table S3. Lattice parameters (a = b, Å) and binding energies (E_b, meV/Å^2) of the heterojunctions. The lattice mismatch for C_2N and MX and the distance (d, Å) between C_2N and MX.

	a	E_b	C_2N	MX	d
C_2N/GaSe	8.14	20.2	-2.2%	8.0%	3.40
C_2N/GaTe	8.28	-10.8	-0.5%	1.2%	3.49
C_2N/InTe	8.39	-9.6	0.8%	-2.9%	3.45

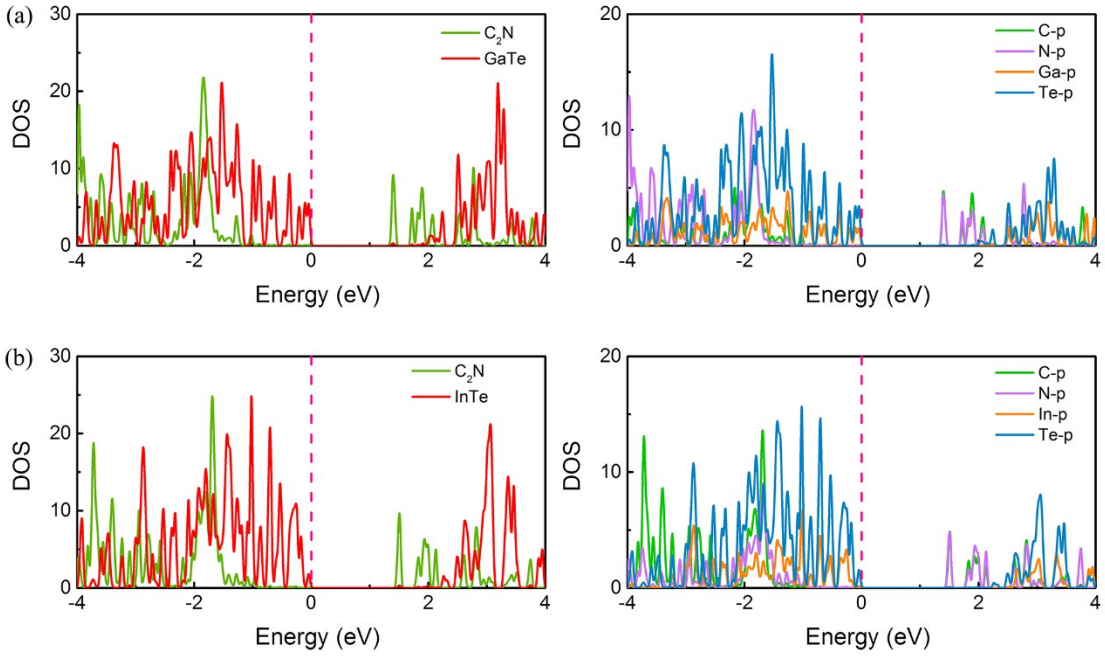

Fig. S4 Partial density of states (PDOS) near Fermi level for (a) C_2N/GaTe and (b) C_2N/InTe.

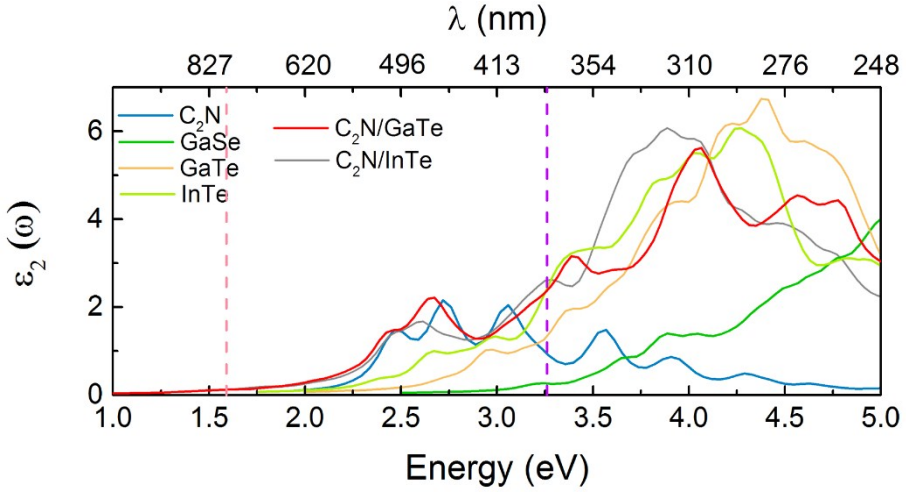

Fig. S5 Imaginary parts of dielectric function for the isolated C_2N, GaSe, GaTe and InTe monolayers as well as C_2N/GaTe and C_2N/InTe heterojunctions. The area between the red and the purple dashed lines represents the visible-light range.

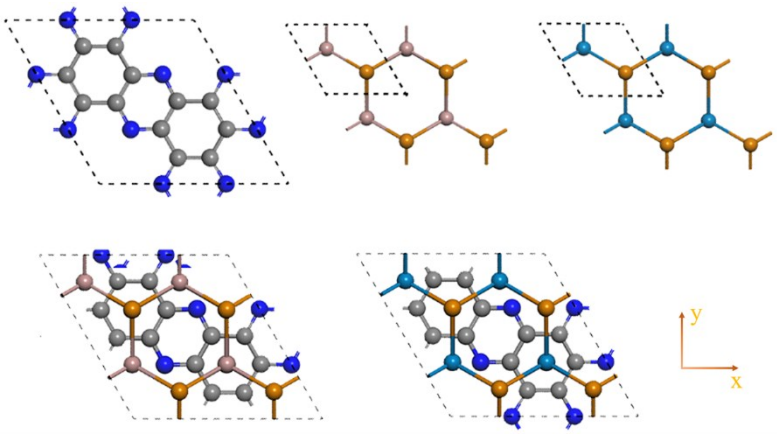

Fig. S6 The x and y directions investigated in this work.

Table S4. Effective mass |m*| (m_e, mass of free electrons), in-plane stiffness C (N m^{-1}), DP constant $|E_1|$ (eV) and carrier mobility μ_{2D} (cm^2 V^{-1} s^{-1}) for electrons and holes for isolated C_2N, GaTe and InTe monolayers along the direction of x and y, respectively.

		|m*|	C	$\|E_1\|$	μ_{2D}
C_2N	e_x	0.46	163.21	1.54	4505.64
	h_x	12.57	163.21	2.71	2.00
	e_y	0.42	162.95	1.90	3631.42
	h_y	7.96	162.95	3.35	3.25
GaTe	e_x	0.13	64.16	11.56	381.90
	h_x	1.30	64.16	2.67	74.75
	e_y	0.57	64.11	1.04	2530.78
	h_y	1.08	64.11	2.88	93.95
InTe	e_x	0.16	48.97	9.71	303.33
	h_x	1.82	48.97	2.58	28.23
	e_y	0.16	48.48	9.70	287.16
	h_y	1.76	48.48	2.85	27.30

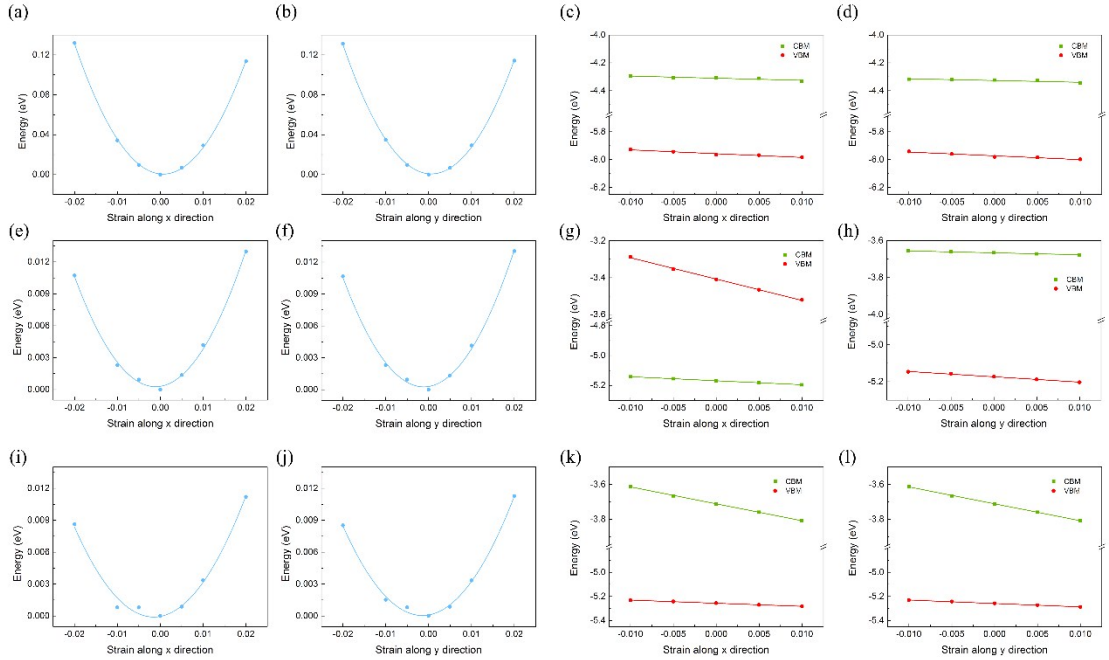

Fig. S7 The relationship between energy and strain for (a,b) C_2N, (e,f) GaTe and (i,j) InTe. The CBM and VBM along the x and y directions as a function of deformation proportion for (c,d) C_2N, (g,h) GaTe and (k,l) InTe.

Table S5. Macroscopic static dielectric constants and the exciton binding energies of isolated C_2N, GaTe and InTe monolayers as well as C_2N/GaTe and C_2N/InTe heterojunctions.

	ϵ_{el}			ϵ_{ion}			E_b
	x	y	z	x	y	z	
C_2N	0.04	0.04	0	2.63	2.63	1.12	1.24
GaTe	0.83	0.83	0	4.11	4.11	1.42	0.27
InTe	1.08	1.08	0.01	3.98	3.98	1.46	0.14
C_2N/GaTe	0.80	0.80	0.02	4.54	4.54	1.45	0.31
C_2N/InTe	0.88	0.88	0.01	4.48	4.48	1.50	0.13

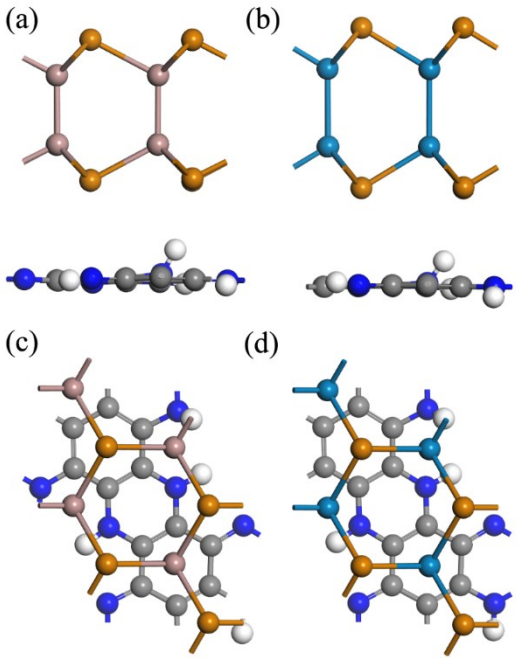

Fig. S8 Side and top view of optimized geometric structures for the fourth hydrogen atom adsorbed on (a,c) C_2N/GaTe and (b,d) C_2N/InTe heterojunctions. The white balls represent hydrogen atoms.